Electronic Supplementary Information

Nanoalloying bulk-immiscible iridium and palladium inhibits hydride formation and promotes catalytic performances

Claudia Zlotea, Franck Morfin, Thanh-Son Nguyen, Nhat-Tai Nguyen, Jaysen Nelayah, Christian Ricolleau, Michel Latroche, and Laurent Piccolo

1. Catalyst preparation procedure

Amorphous silica-alumina (ASA, commercial name SIRAL) was supplied by SASOL (formerly CONDEA), following a patented preparation procedure.[1,2] SIRAL-40, containing 40 wt.% silica, was chosen as a support for its optimal performances in tetralin hydroconversion, in correlation to its Brönsted acidity.[3] The powder, received in hydrated form, was activated by heating at 550°C in air for 3 h. It resulted in dehydration and transformation of the alumina part from AlO(OH) (boehmite) to γ-Al_2O_3. For SIRAL-40, the average oxide grain size, BET surface area, pore volume and pore diameter were 50 µm, 500 m^2 g^{-1}, 0.90 mL g^{-1} and 6.4 nm, respectively.

The catalysts were prepared by incipient wetness (co-)impregnation of the supports with Ir acetylacetonate, $Ir(acac)_3$, and/or Pd acetylacetonate, $Pd(acac)_2$. These precursors (SIGMA-ALDRICH, purity 97%) were dissolved in toluene. After maturation during 2 h at room temperature, the samples were dried at 120°C overnight and reduced in an H_2 flow (60 mL/min) at 350-550 °C for 6 h (heating ramp 2 °C/min). In the case of Ir/ASA, it has been shown that the catalysts must be treated by direct H_2 reduction of acac-impregnated ASA, without pre-calcination, to avoid particle agglomeration.[4]

The metal loadings were determined from inductively coupled plasma - optical emission spectrometry (ICP-OES, Activa – HORIBA JOBIN YVON).

Table S1. Characteristics of the samples.

	Metal loading (wt%)[a]	V_{ads} (cm³/g)[b]	Dispersion (%)[c]	Mean size (nm)[d]	Mean size (nm)[e]
Pd/ASA	0.89	24.7	23.5	4.7	4.5 ± 1.2
Ir/ASA	2.5	37.5	64.3	1.7	1.5 ± 0.3
IrPd/ASA	4.5	37.3	49.4	2.2	2.2 ± 0.8

[a] Determined from ICP-OES; [b] Adsorbed volume determined from irreversibly chemisorbed oxygen extrapolated at zero pressure limit; [c] Metal dispersion derived from V_{ads} using O:metal stoichiometry of 1; [d] Mean particle diameter determined from 1.1 nm/dispersion; [e] Sauter mean particle diameter determined from TEM.

2. Transmission electron microscopy and energy-dispersive X-ray spectroscopy

To study the structure, morphology and composition of the metal particles by (scanning) transmission electron microscopy ((S)TEM), the catalysts were transferred onto a standard TEM grid (holey carbon on a 400 mesh Cu grid, AGAR SCIENTIFIC). In some cases, carbon replicas of the catalysts were prepared in order to facilitate the imaging of the smallest nanoparticles.

Aberration-free high resolution transmission electron microscopy (HRTEM) imaging, STEM high-angle annular dark-field (STEM-HAADF) imaging and energy-dispersive X-ray (EDX) spectroscopy were undertaken with a JEOL Cold-FEG JEM-ARM 200F microscope equipped with a highly coherent and bright cold field-emission electron source and with a CEOS CESCOR hexapole aberration corrector to compensate the spherical aberration of the objective lens.[5] In order to avoid beam-induced nanoparticle

modifications, the microscope was operated at an accelerating voltage of 80 kV with the emission current set to 20 µA. Even at an acceleration voltage of 80 kV, the combination of the cold FEG and the spherical aberration correction produced directly interpretable HRTEM images with 80 pm resolution (and below 75 pm at 200 kV). STEM-HAADF imaging was achieved using a JEOL annular dark-field detector with large inner and outer collection angles set to 68 and 280 mrad, respectively. The probe size setting was 8C, and a 40 µm condenser lens aperture was used. The nanoparticle composition was determined by (S)TEM-EDX spectroscopy of single nanoparticles. TEM-EDX analyses were undertaken with a nanobeam of 2.4 nm while STEM-EDX was achieved with a sub-nm probe (probe size setting 5C or 6C). X-rays were collected by a JEOL detector (EX-24063JGT). The acquisition time was either 50 s or 100 s to allow for sufficient counting statistics necessary for reliable quantification. Instead of using a fixed probe, the electron beam was continuously scanned in a controlled manner over a rectangular region on the NPs during STEM-EDX measurements (for each particle, the scanned region was chosen to encompass its projected area). This minimized electron beam-induced damage and ensured accurate NP composition measurement. The latter was determined by analyzing the intensities under the Ir-$M_{\alpha,\beta}$ (1.86-2.86 keV range) and Pd-$L_{\alpha,\beta}$ (2.70-2.97 keV range) edges using the Cliff-Lorimer method.[6] The experimental K-factor was determined from global analysis of the sample, knowing its overall composition ($Ir_{49}Pd_{51}$) from ICP-OES. Some other TEM observations were also performed with a JEOL JEM-2010 conventional TEM (see Fig. 1a in the main article).

Figure S1 displays STEM-HAADF images of the Ir-Pd/ASA catalyst. Because of the higher atomic number of Ir and Pd as compared to the constituent elements of the amorphous support, the metal nanoparticles display the brightest HAADF intensity. This contrast difference between the support and the metallic phase makes particle identification and characterization quite straightforward. From the image in (b), it can be deduced that the majority of the synthesized nanoparticles have in-plane sizes between two and three nanometers. In addition, some bigger particles with sizes extending up to about 10 nm are present in the sample.
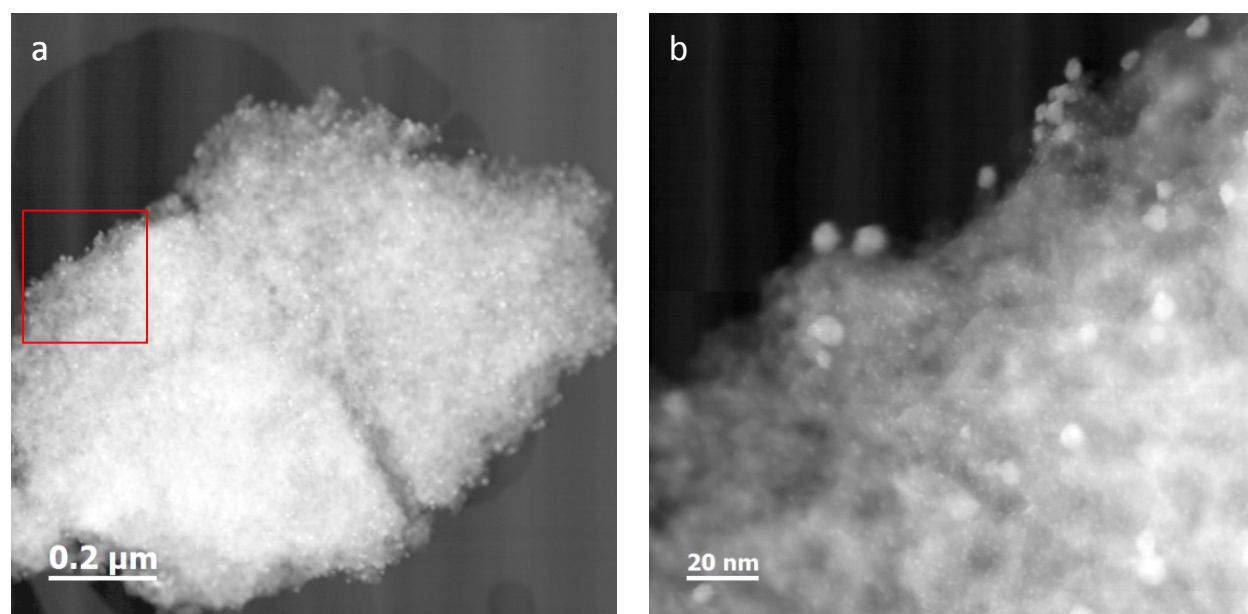
Figure S1. STEM-HAADF images of Ir-Pd nanoparticles supported on amorphous silica-alumina(ASA). (a) Low-magnification image showing the ASA support with the brighter intensity spots corresponding to the largest Ir-Pd nanoparticles. (b) Image of the region enclosed in red in (a). Most of the nanoparticles have sizes around 3 nm or less, and are visible in (b). Few nanoparticles with sizes above 6 nm are clearly visible on both images.
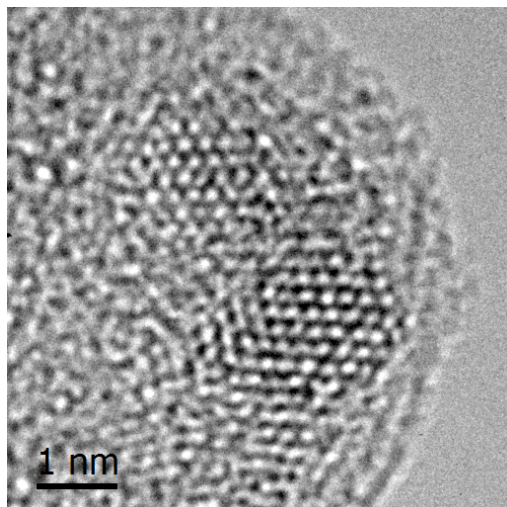
Figure S2. HRTEM image of two Ir-Pd nanoparticles with sizes below 2 nm.

Figure S2 shows an aberration-free HRTEM image of two Ir-Pd nanoparticles on the ASA support. These metallic particles are representative of the smallest ones observed in the prepared catalyst. This HRTEM image clearly shows the crystalline nature of these small entities.

Figure S3a shows the variation of the composition as a function of the in-plane size obtained by analyzing 19 particles with size ranging from 2 to 11 nm. Due to the limited counting statistics for nanoparticles in the size range probed, the composition uncertainty was fixed to 10% for all measurements. The uncertainty in the measurement of the in-plane size was estimated by measuring the size of each particle in two perpendicular directions, with the in-plane size being equal to the mean of these values and the associated uncertainty equal to the highest deviation from the mean value. The experimentally-determined size-composition relationship in the Ir-Pd nanoparticles shows a clear enrichment in Pd as particle size increases. In particular, the particles with sizes below 2 nm are mostly Ir-pure, whereas the largest ones, with sizes exceeding 6 nm, display compositions around $Ir_{20}Pd_{80}$. This size-composition correlation is consistent with previous observations.[7]

Figure S3b shows a dark-field image of an assembly of Ir-Pd NPs with the STEM-EDX spectrum from the NP marked 008. The size of this NP is 5.1 ± 0.4 nm with a composition equal to 52.7 at% Ir.
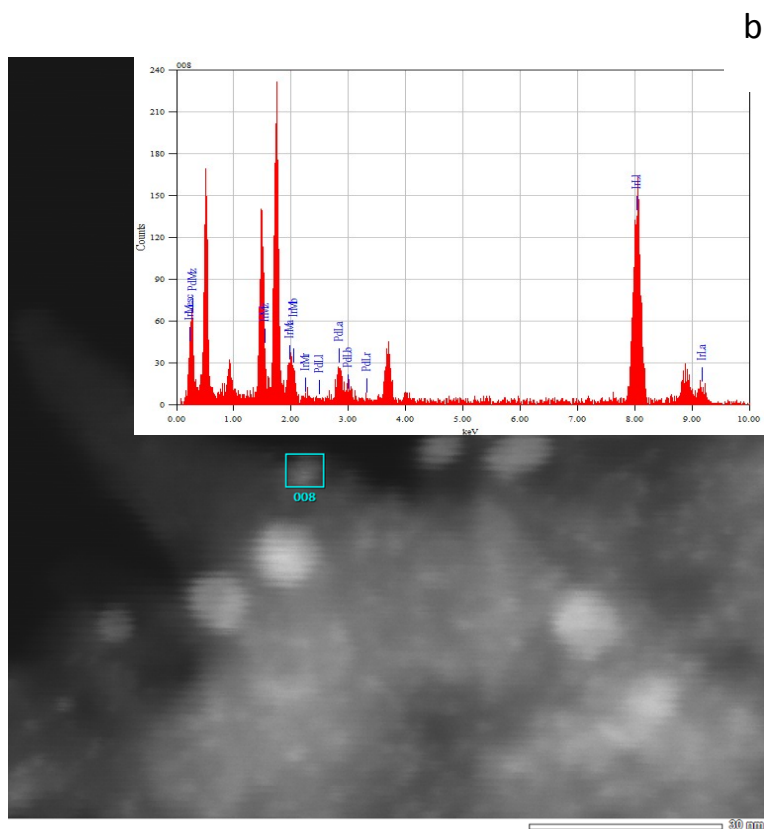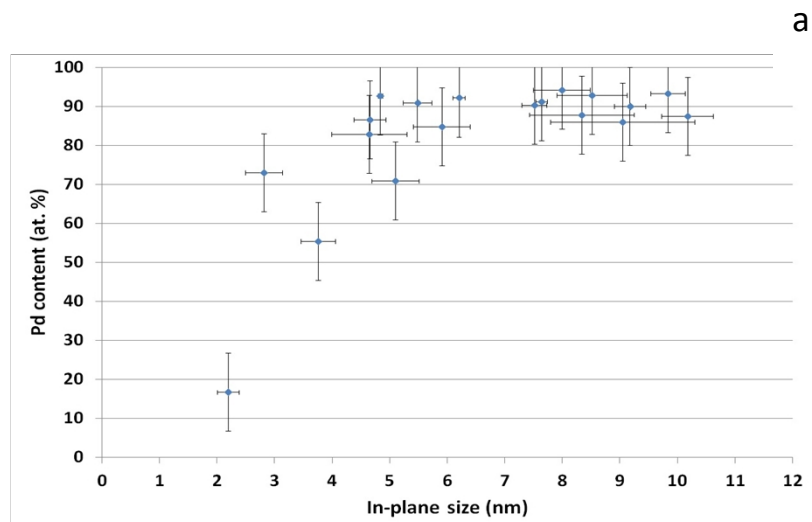
a

b

Figure S3. (a) Size-composition relationship in the ASA-supported Ir-Pd nanocatalysts. As the size of the particles increases, they become richer in Pd, with the largest ones having compositions around $Ir_{20}Pd_{80}$. The size-composition correlation in the 1-6 nm size range is similar to that obtained for other Ir-Pd/ASA catalysts with lower metal loading (0.9 wt% vs 4.5 wt% here).[7] (b) Example of STEM image, and EDX spectrum for the NP squared by a blue line.

Spatially resolved EDX spectroscopy was performed in STEM mode using a 5C probe diameter (0.7 nm) and 1.1 nm linear steps. At each step, the spectrum recording time was 50 s. An example of spectra series is given in Figure S4.
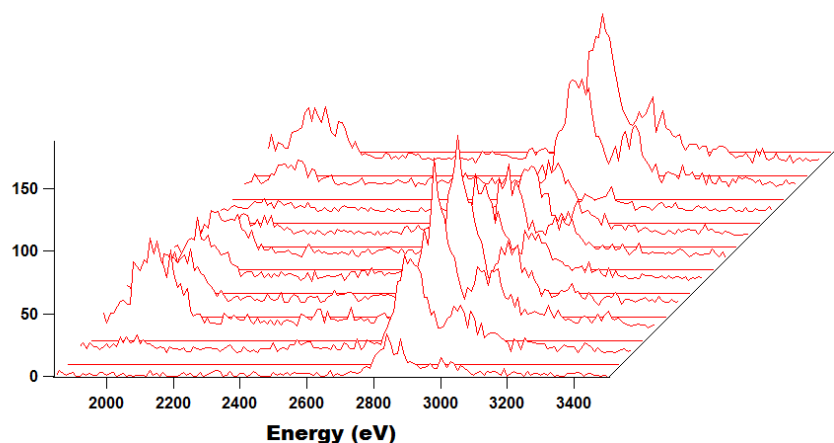

Figure S4. Series of spatially-resolved EDX spectra corresponding to Fig. 1e. Peaks at the left and right-hand sides correspond to Ir-M and Pd-L edges, respectively.

3. X-ray diffraction

Structural characterization by powder X-ray diffraction (XRD) was performed using a D8 Advance BRUKER diffractometer (Cu K_α radiation). The XRD patterns of ASA, Pd/ASA, Ir/ASA and IrPd/ASA are shown in figure S4. The FWHM of diffraction peaks from silica-alumina are very broad, indicating a mostly amorphous oxide support, although containing some γ-alumina phase.[4] The diffraction lines from metallic nanoparticles are not visible, in agreement with the small amount of active phase in the samples and the small particle sizes. The positions of the main diffraction lines of pure fcc Pd and Ir are also indicated.
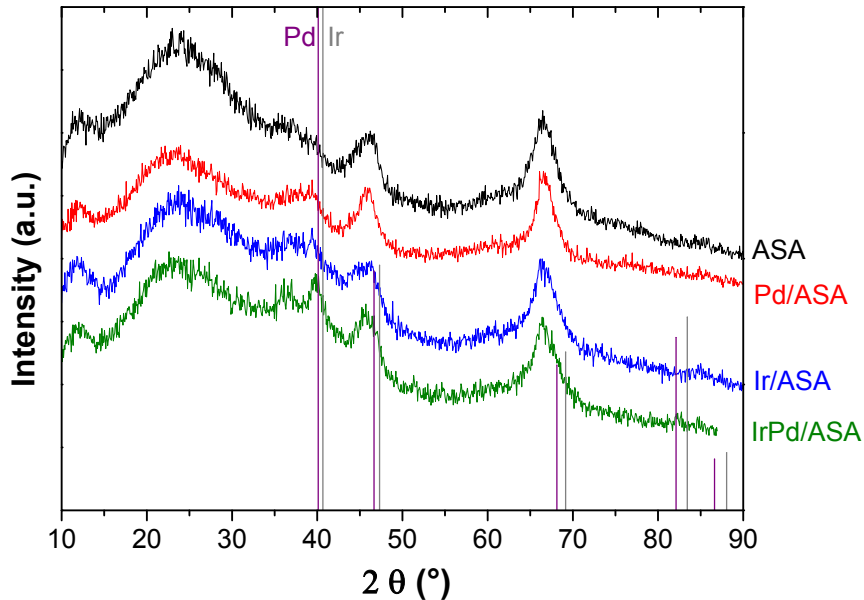
Figure S5. XRD patterns of ASA, Pd/ASA, Ir/ASA and IrPd/ASA

4. Hydrogen sorption by volumetric method (protocol I)

Hydrogen sorption properties were determined by measuring the Pressure-Composition Isotherm (PCI) at 25 °C up to 0.1 MPa hydrogen pressure using an automated volumetric device (QUANTACHROME Autosorb IQ). The pre-conditioning of the samples consisted of three successive cycles of reduction under H_2 atmosphere (up to 0.1 MPa) and degassing under secondary vacuum at 120 °C. The PCI curves were recorded by stepwise increase/decrease (sorption/desorption) of hydrogen pressure. They were measured several times (each time preceded by outgassing) with good measurement repeatability. Figure S5 shows two consecutive measurements for Pd/ASA, Ir/ASA and IrPd/ASA samples. For Pd/ASA, the second measurement has been performed up to 0.01 MPa. The curves are expressed as volume of absorbed/desorbed H_2 (cm^3/g of catalyst) vs. equilibrium H_2 pressure.
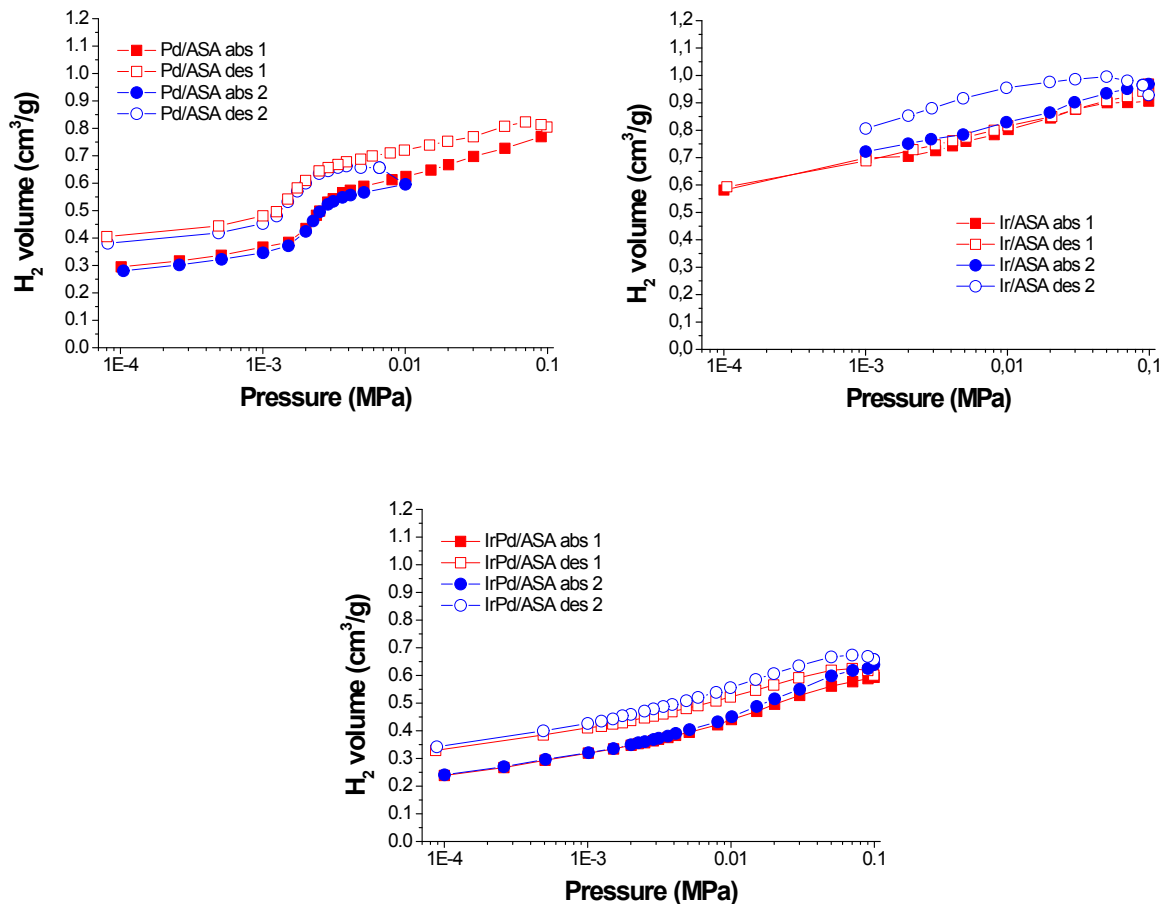
Figure S6. Measurement repeatability of the PCI curves for Pd/ASA, Ir/ASA and IrPd/ASA catalysts (25 °C).

5. Oxygen and hydrogen chemisorption measurements (protocol II)

5.1. Experimental

An homemade volumetric adsorption apparatus described elsewhere[8] was used to perform oxygen and hydrogen chemisorption measurements. The samples were pretreated by cycles of reduction (1 atm H_2) and evacuation at temperatures up to 300 °C, followed by a final evacuation at 300 °C under secondary vacuum overnight.

For the adsorption measurements at 30 °C, the pressure of H_2 or O_2 was increased step by step (with volumetric analysis at each step) on the pretreated sample ("total adsorption", V_{tot}). Then the sample was evacuated under vacuum for 2 h at the measurement temperature, and the stepwise pressure increase/adsorption measurement was performed again ("reversible adsorption", i.e., physisorption, V_{rev}). The "irreversible adsorption" (i.e., chemisorption) contribution is $V_{irrev} = V_{tot} - V_{rev}$. Note that hydrogen absorption, if any, is included in V_{rev}.

The metallic dispersion (number of surface atoms / total number of atoms) was derived from the numeric fit of the linear part (50-300 mbar range in our case) of $V_{irrev}(P_{O2,eq})$, taking the intersection between Y axis and the fitting line.[8] In our case, we assumed an adsorption stoichiometry of 1 ($O_{irrev}:M_{surf}$ = 1, where M = Ir or Pd).[9] For calculating the mean nanoparticle size corresponding to the measured dispersion, we used: *size* [nm] = 1.1 / *dispersion*. This formula is valid for Pt-group metals and spherical or truncated-cuboctahedral particles larger than ca. 1.5 nm. [10]
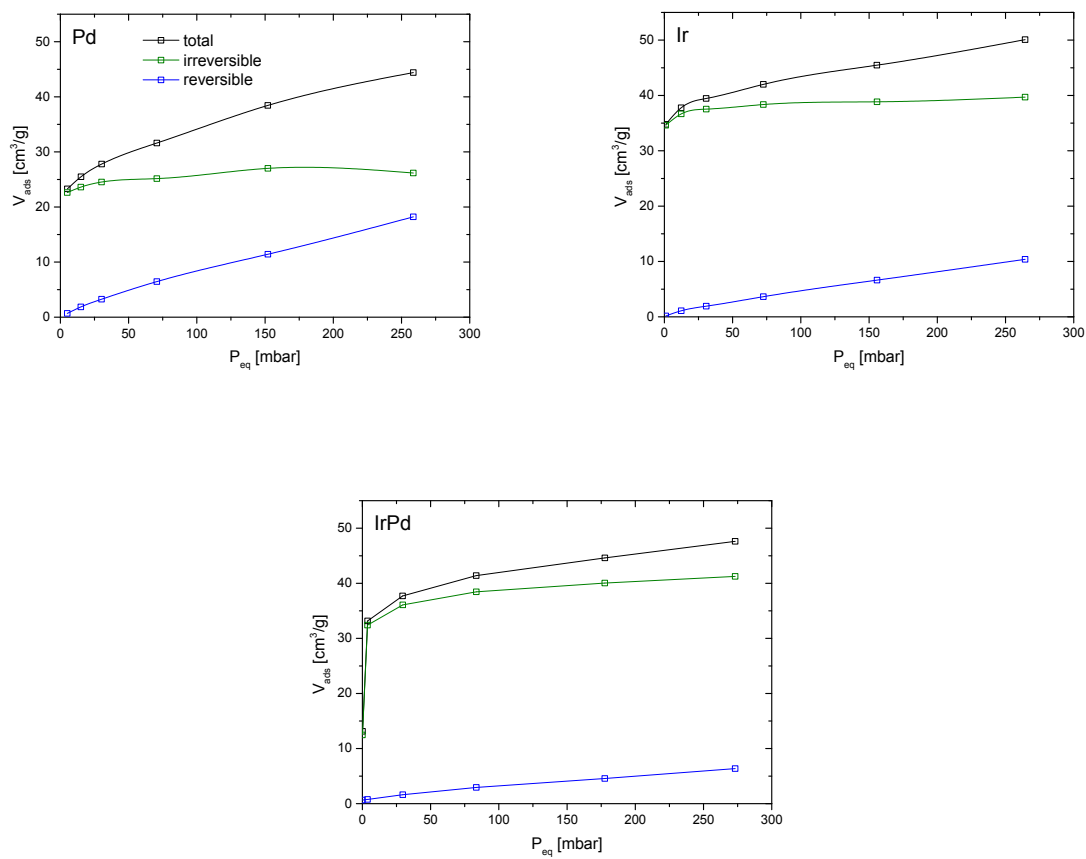
5.2. Oxygen

Figure S7. Oxygen adsorption isotherms at 30 °C for ASA-supported samples.

The volumes of irreversibly adsorbed oxygen used for dispersion measurements are reported in Table S1.
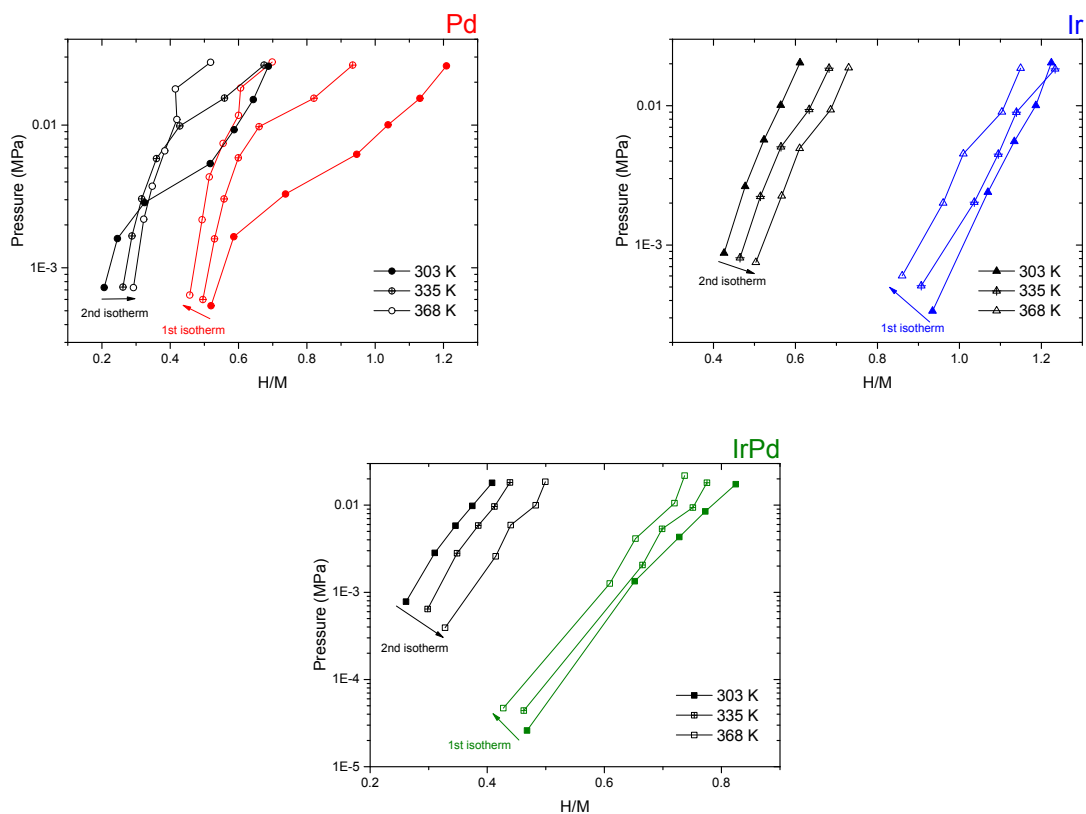
5.3. Hydrogen

Figure S8. Hydrogen sorption isotherms at 30, 62, and 95 °C plotted as PCI curves (as in Fig. 2 and Fig. 3, *H/M* is the number ratio of adsorbed hydrogen atoms and metal atoms).
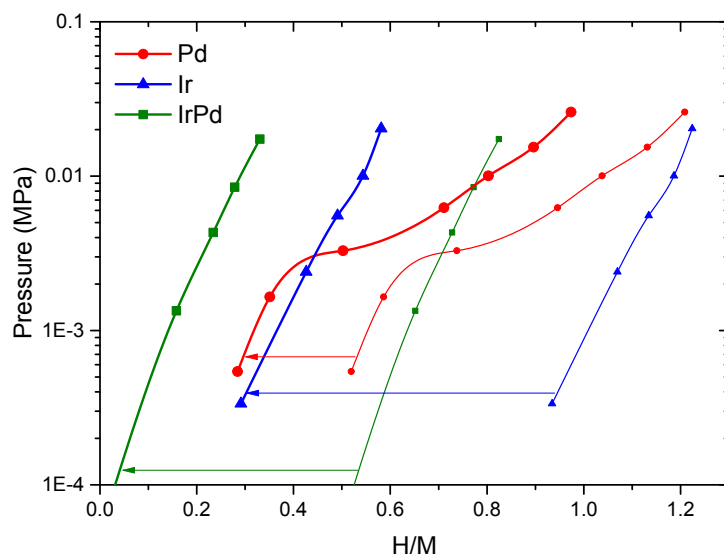
Figure S9. Hydrogen sorption isotherms at 30 °C plotted as PCI curves. Small and large symbols correspond to "*total adsorption*" and dispersion-corrected data (H/M-M_{surf}/M where the metal dispersion M_{surf}/M was obtained from oxygen chemisorption measurements), respectively.

6. Catalysis

Each catalyst was evaluated in two reactions: the oxidation of CO and the selective oxidation of CO in the presence of H_2 (PROX). These tests were carried out at atmospheric pressure and variable temperature in a continuous flow fixed-bed reactor. The catalysts were diluted in Al_2O_3 (CONDEA Puralox ScFa-215) in order to obtain a catalytic bed of 800 mg (height of 13 mm in the quartz U-shaped 10 mm-diameter tubular reactor). The reactant gases were mixed using mass-flow controllers (BROOKS INSTRUMENTS) and flowed through the reactor at a total rate of 50 Nml min^{-1}. All the high-purity (> 99.995%) gases were purchased from AIR LIQUIDE. The gas mixture consisted of 2 % CO + 2 % O_2 + 96 % He for CO oxidation, and 2 % CO + 2 % O_2 + 48 % H_2 + 48 % He for PROX. The outlet gases were analyzed online using a VARIAN Micro GC (CP2003).

The following test sequence was used for all samples: in-situ reducing pretreatment, CO oxidation, and PROX. The pretreatment consisted in heating the catalyst under hydrogen flow (50 ml min^{-1}) from room temperature (RT) to 400°C at a rate of 3°C min^{-1}, followed by 2 h plateau at 400 °C. The CO oxidation and PROX experiments consisted of two heating-cooling cycles (50-350-50°C) at a rate of 80 °C h^{-1}. Only the last (cooling) reaction runs are shown in Figures 3 (conversions), S10 (turnover frequencies), and S11 (selectivities).
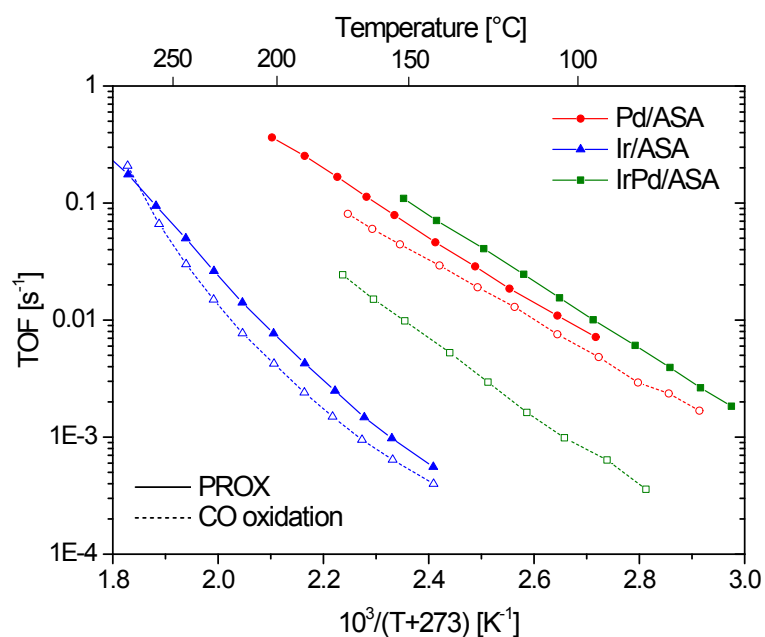

Figure S10. Arrhenius plot of the catalyst turnover frequencies (CO_2 molecules formed per second per surface metal atom) for CO oxidation and PROX. They were derived from the flow rate and the conversion values in Fig. 3, taking the sample characteristics in Table S1 into account. Only the (quasi) linear part of the data, corresponding to low CO conversions (< 20% in most cases), is plotted. The activation energies derived from numeric fits range between 21 kJ mol^{-1} (CO oxidation on Pd/ASA) and *ca*. 40 kJ mol^{-1} (CO oxidation on Ir/ASA).
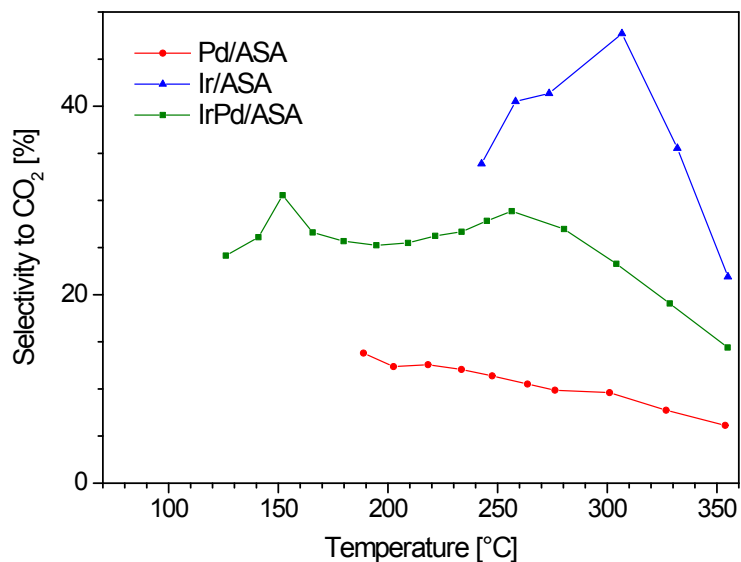
Figure S11. Catalyst selectivities in PROX.

References

(1) Meyer, C.; Noweck, K.; Reichenauer, A.; Schimanski, J. Process for the preparation of a catalyst carrier based on aluminosilicates. US5045519, 1991.

(2) Daniell, W.; Schubert, U.; Glöckler, R.; Meyer, A.; Noweck, K.; Knözinger, H. *Appl. Catal. Gen.* **2000**, *196*, 247.

(3) Nassreddine, S.; Casu, S.; Zotin, J. L.; Geantet, C.; Piccolo, L. *Catal. Sci. Technol.* **2011**, *1*, 408.

(4) Nassreddine, S.; Bergeret, G.; Jouguet, B.; Geantet, C.; Piccolo, L. *Phys. Chem. Chem. Phys.* **2010**, *12*, 7812.

(5) Ricolleau, C.; Nelayah, J.; Oikawa, T.; Kohno, Y.; Braidy, N.; Wang, G.; Hue, F.; Florea, L.; Bohnes, V. P.; Alloyeau, D. *Microscopy* **2013**, *62*, 283.

(6) Cliff, G.; Lorimer, G. W. *J. Microsc.* **1975**, *103*, 203.

(7) Piccolo, L.; Nassreddine, S.; Aouine, M.; Ulhaq, C.; Geantet, C. *J. Catal.* **2012**, *292*, 173.

(8) Morfin, F.; Sabroux, J.-C.; Renouprez, A. *Appl. Catal. B Environ.* **2004**, *47*, 47.

(9) Paryjczak, T.; Szymura, J. A. *Z. Für Anorg. Allg. Chem.* **1979**, *449*, 105.

(10) Bergeret, G.; Gallezot, P. In *Handbook of heterogeneous catalysis*; G. Ertl, H. Knözinger, J. Weitkamp (Eds.): Weinheim, 1997.